Volume 3 Issue 1 (March 2023)
DOI 10.24191/jaeds.v3i1.52
eISSN 2805-5756

Journal of Applied Engineering Design & Simulation

Simulation of Surface Crack Interaction of Marine Solid Shaft

Noor Elya Nashiewa Shabarudin[1], and Muhammad Hussain Ismail[1,2*]
[1]Industrial Metallurgy Research Group (IMReG), School of Mechanical Engineering, College of Engineering, Universiti Teknologi MARA, Shah Alam 40450 Selangor, Malaysia.
[2]Smart Manufacturing Research Institute (SMRI), Universiti Teknologi MARA, Shah Alam 40450 Selangor, Malaysia.
*corresponding author: hussain305@uitm.edu.my

ABSTRACT

The marine industry relies on the transmission of power through a propeller shaft, which is typically a solid cylinder. However, when cracks appear in the shaft's hub, it is crucial to take preventative measures to avoid failure. Solid cylinders are susceptible to cracking and fracturing under various mechanical stresses, leading to single or multiple cracks. The interaction between these fractures can significantly impact the structure's collapse, and thus, this study aims to address the issues that emerge from the interaction of multiple cracks under specific loading conditions. To achieve this goal, research on various crack configurations on the cylinder's surface using finite element software, Ansys™ has been conducted to calculate the stress intensity factor (SIF) under different types of loading. The cylinder's dimensions were set to 200 mm in length and 50 mm in diameter, while the crack depth ratio ranged from 0.1 to 0.4, with an increment of 0.1. The crack aspect ratio was set to 0.6. The results were normalized to generalize the interaction factor and the relationship between two cracks and a single crack. It was found that the interaction factor is dependent on the separation distance between the cracks and the crack depth ratio. These findings suggest that preventative measures should be taken to mitigate the risks of crack formation and interaction, such as regular inspections and maintenance.

Keywords: stress intensity factor, crack interaction, surface crack

Nomenclature (Greek symbols towards the end)

A	Area of solid shaft cylinder (m^2)
σ	Stress of loading (MPa)
a	Crack depth (m)
b	Crack length (m)

Abbreviations

AE	acoustic emission
FEA	finite element analysis
FEM	finite element method
HFO	heavy fuel oil
KI	stress intensity mode II
KII	stress intensity mode II
KIII	stress intensity mode III
SIF	stress intensity factor

1.0 INTRODUCTION

During the early nineteenth century, the rise of steam engines marked the beginning of a new era in ship engineering. The challenge for designers was to find a way to efficiently transfer power from the engine inside the hull to the ship's working parts. The engine room is often considered the heart of the vessel, as it drives the massive marine engines that power the vessel to travel at speeds of up to 50 kmph using diesel oil or HFO [1]. In most ships, the engine is located in the middle, which necessitates a long propeller shaft line to transmit power to the stern through a tunnel to maintain the ship's balance. The propulsion system of a ship is critical, as it converts rotational velocity into translational momentum to propel the vessel. Propellers and other mechanical propulsion systems generate thrust, which is essential for ships to move forward. This mechanism involves an engine attached to a shaft that propels the propeller. A typical marine propulsion system consists of a main engine, marine shaft, driving device, and propeller, as shown in Fig.1[2].

Received on 29.08.2022
Accepted on 24.03.2023
Published on 29.03.2023

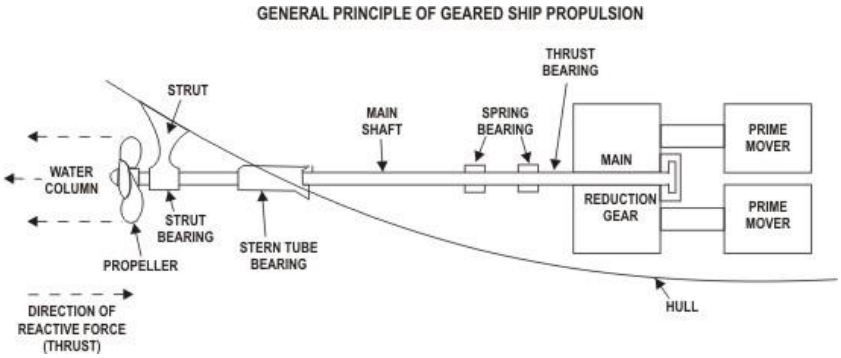

Figure 1. General principle of Geared Ship Propulsion [2]

The propeller shaft, also known as the marine shaft, is a critical mechanical component that transmits power from a vessel's hull-mounted engines to its aft propellers. It functions similarly to driveshafts in automobiles, transferring rotational power from the engine to the propellers. The marine shaft is an essential part of any propulsion system, which is any mechanical device that generates forward motion. As mentioned in [3], the propeller shaft is typically a solid cylindrical structure made of durable metallic materials chosen by naval architects for their strength and ability to withstand high-stress situations. This is because the shaft must withstand the tremendous forces generated by the engine's power as it rotates. Overall, the propeller shaft is a crucial element in the functioning of a ship's propulsion system, and its construction must be carefully designed to ensure reliable operation even in challenging marine conditions.

Shaft failure analysis is often perceived as a complex and expensive process, but this is a common misunderstanding. The propulsion shaft in a ship is exposed to a range of stresses, including torque, bending, axial thrust, and transverse stress from gravitational and centrifugal forces, during operation. The propulsion system operates in a harsh environment that is exposed to salt or oil mist, and there are often long periods of inactivity lasting several months with variable load amplitudes. These factors increase the risk of propulsion system failure due to sea and weather conditions. As cited in [4][5], the fatigue behaviour and longevity of the shaft are influenced by several factors. These include the material used in the shaft's construction, the shaft's design and manufacturing quality, and the operating conditions that the shaft is exposed to. Other factors such as maintenance practices and operating procedures can also impact the shaft's performance. It is crucial to conduct regular inspections and testing of the propulsion shaft to ensure it is functioning correctly and to identify any potential issues early on. This can help prevent costly and time-consuming repairs and reduce the risk of failure during critical operations. By understanding the various factors that affect the propulsion shaft's performance, engineers can take proactive measures to maintain and optimize its operation, ensuring the safe and efficient operation of the vessel.

As noted by the author in [6], catastrophic failures often occur unexpectedly due to significant fractures, cracks, or defects resulting from cyclical loads, material faults, or manufacturing defects. In the case of a propulsion shaft failure, it may start to crack in several areas, indicating that the shaft is not straight due to numerous ratchet marks on both the top and bottom of the shaft [7]. Fractures generally appear at a 90-degree angle to the plane of maximum stress unless stated otherwise. In many cases, crack initiation and propagation occur more commonly during bending stress rather than torsion, although this may not always be the case, particularly for shafts subjected to high torsion stress.

Figure 2. Example of transverse crack on solid shaft in Marine.

1.1 Stress intensity factor

The difficulties in addressing fracture mechanics cannot be solved analytically; therefore, numerical methods such as finite element analysis are used. This approach is particularly useful in calculating the stress intensity factor (SIF), a critical parameter in analysing fracture structures in mechanical systems. Recent research has focused on predicting the SIF by studying cracks in cylindrical components, particularly in shafts, where surface cracks are the most common cause of failure (Mode I) [7][8].

To minimize computation time, previous authors have reported that the crack front shape remains constant during the fatigue growth phase [9]. When using the finite-element technique, it is assumed that the component geometry is parametric, and the most common shapes used are circular and elliptical arcs. The nomenclature for elliptical surface cracks is illustrated in Fig. 3. By accurately predicting the SIF, engineers can estimate the rate and direction of crack growth and develop mitigation strategies to prevent catastrophic failures. Therefore, finite element analysis is an essential tool for ensuring the structural integrity and safe operation of mechanical systems, particularly those subjected to cyclic loading and stress.

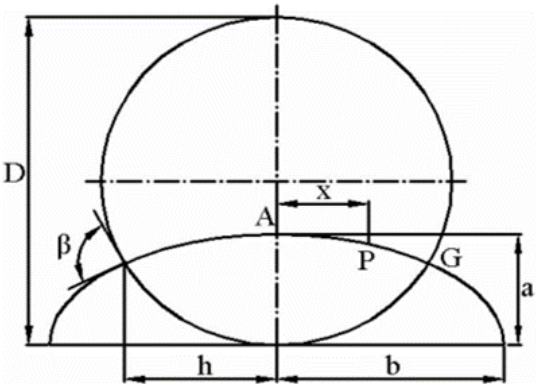

Figure 3. Arbitrary crack shape[10]

2.0 METHODOLOGY

2.1 Benchmarking modelling

To accurately study the behaviour of surface cracks under different stress levels, a scale model is constructed according to accepted dimensions. These dimensions are based on current research and are widely used in the field. The model is made of Medium Carbon Steel, which is commonly used in maritime settings. Fig.4 illustrates the solid shaft model with dimensions of 200mm x 50mm, as determined by previous studies.

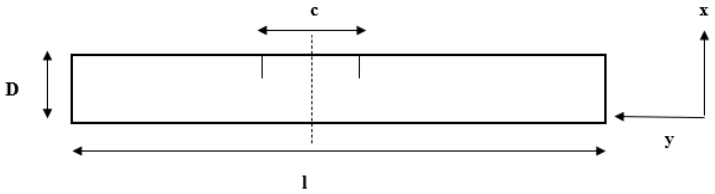

Figure 4. The layout of the crack.

2.2 Develop finite element modelling

Fig.5 shows a schematic representation of the solid finite element (FE) model used in the study. The model is made of carbon steel, with a length of 200mm and a thickness of 50mm, as determined by previous research [11]. The Poisson ratio is assumed to be 0.29, and Young's modulus is set to 200GPa. These values are chosen based on the material properties of carbon steel and are necessary inputs for the FE analysis.

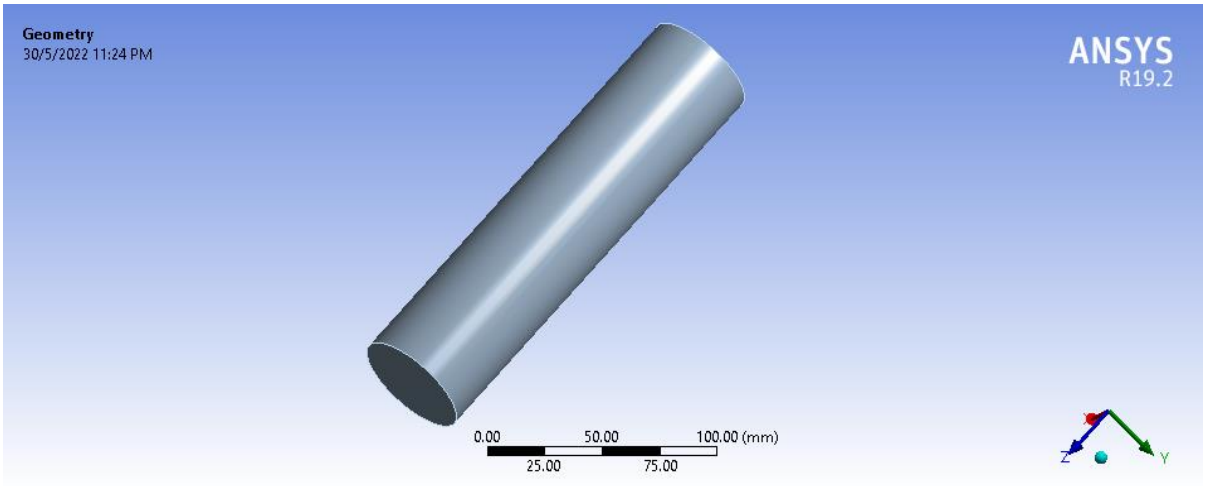

Figure 5. Solid cylindrical shaft in Ansys Design Modeler.

2.3 Crack configurations

The present study focuses on analysing a parallel crack located on the exterior surface of the cylinder. The crack's morphology and behaviour under different stress conditions are investigated in detail. For a parallel crack, where $\alpha = 0$, the reference point for the crack's starting coordinates are (0, 25) in the X and Y directions, respectively.

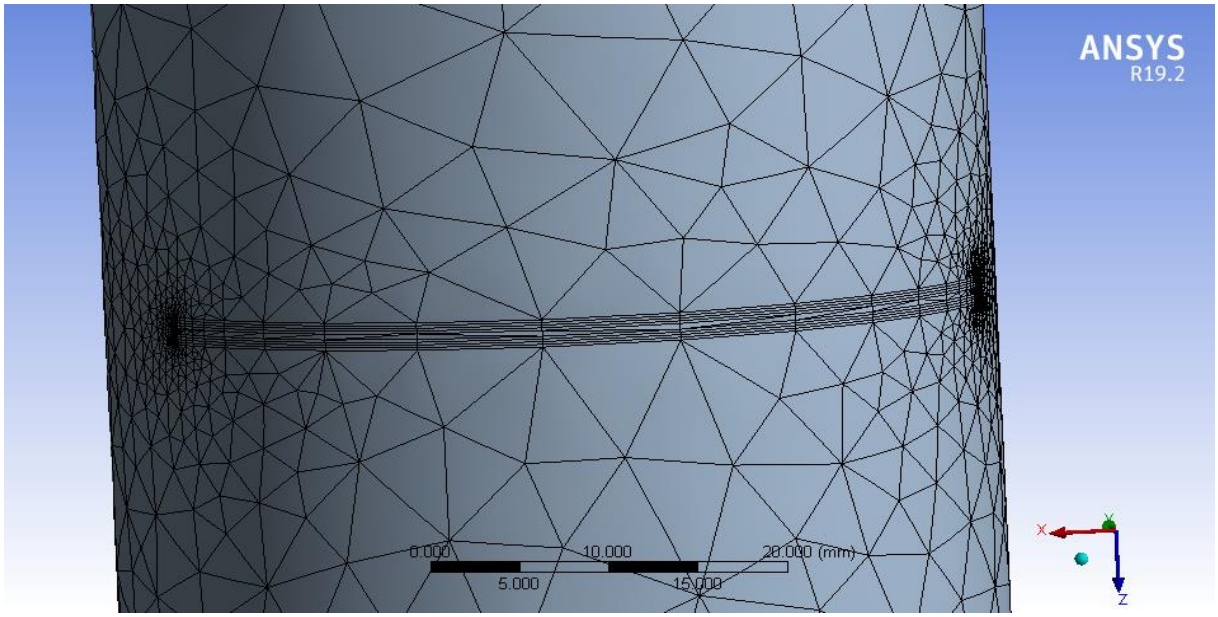

Figure 6. Close view of parallel crack configurations

2.4 Crack parameters

To locate cracks in the ANSYS Mechanical model, a coordinate system is used, with the X-axis indicating the horizontal position and the Y-axis indicating the vertical position of the cracks on the cylinder's face. The separation between the fractures in the cylinder is represented by the distance along the Z-axis, with a fixed value of z=0 for the reference crack and varying values of 1, 2, 4, 8, 16, 32, and 64 for the observed crack, corresponding to separation distance c/l values of 0.005, 0.01, 0.02, 0.04, 0.08, 0.16 and 0.32.

To introduce semi-elliptical cracks into our study, fracture tool is utilized. The major radius of the semi-elliptical crack represents the horizontal radius (b), while the minor radius represents the vertical radius (a). The crack depth ratio (a/D) and the crack aspect ratio (a/b) listed in Table 1 are used in the present study. These values are determined based on the definitions of geometrical parameters agreed upon by Shin and Cai [12].

Table 1: The variables and constant used in this study for observed crack

Crack Aspect ratio, a/b	Crack depth ratio, a/D	Crack depth, a (mm)	Crack Length, b (mm)
0.6	0.1	5.0	8.33
	0.2	10.0	16.67
	0.3	15.0	25.00
	0.4	20.0	33.33

2.5 Normalization of Stress Intensity Factor (SIFs)

To analyse the results, the stress intensity factor (SIF) values from ANSYS simulation are tabulated and then normalized. The normalization process makes it easier to compare the SIFs between different cracked structures by removing the geometrical effects. This aids in the comparison process and ensures the generality of the results. All of the SIFs acquired during the analysis are normalized to enhance the generalizability of the results. For example, a normalized SIF, F, may be described as follow: [10]:

$$(K)SIF = F\sigma\sqrt{\pi} \tag{1}$$

For tension force,

$$Ft = \frac{k}{\sigma\sqrt{\pi a}}, \text{ where } \sigma = \frac{F}{A} \tag{2}$$

$A = 2\pi rh$, area of cylinder of the shaft

For bending force,

$$Fb = \frac{k}{\sigma\sqrt{\pi a}} \text{ where } \sigma_b = \frac{my}{I} \tag{3}$$

$$I = \frac{1}{2}Mr^2$$

For torsion Force,

$$FTor = \frac{k}{\tau\sqrt{\pi a}} \text{ where } \tau = \frac{Tr}{J} \tag{4}$$

$$J = \frac{\pi D^4}{32}$$

For mixed-mode loading,

$$FEqv = \sqrt{(F_I)^2 + (\lambda F_{II})^2 + (\frac{\lambda F_{III}}{1-\nu})^2} \tag{5}$$

Where v= Poisson ratio and $\lambda = \tau/\sigma$b

Where a, D, R, and y are crack depth, shaft outside diameter, distance between axis and the rotation mass and vertical distance from neutral axis.

3.0 RESULTS AND DISCUSSION

In this section, the ultimate outcomes and data obtained from the simulation have been examined and discussed. To achieve the objectives of the study, it is necessary to consider the significance of the outcomes and data by addressing the stress intensity factors.

3.1 Interaction Analysis for Single and Multiple Parallel Cracks of Tension

A tension force of 15000N is applied to the solid shaft with various geometrical parameters as shown in Fig 7. The interactions of surface cracks on the solid shaft are compared with different crack depths and lengths at the Z-axis, with the reference crack at Z=1 or the separation distance, c/l, of 0.005.

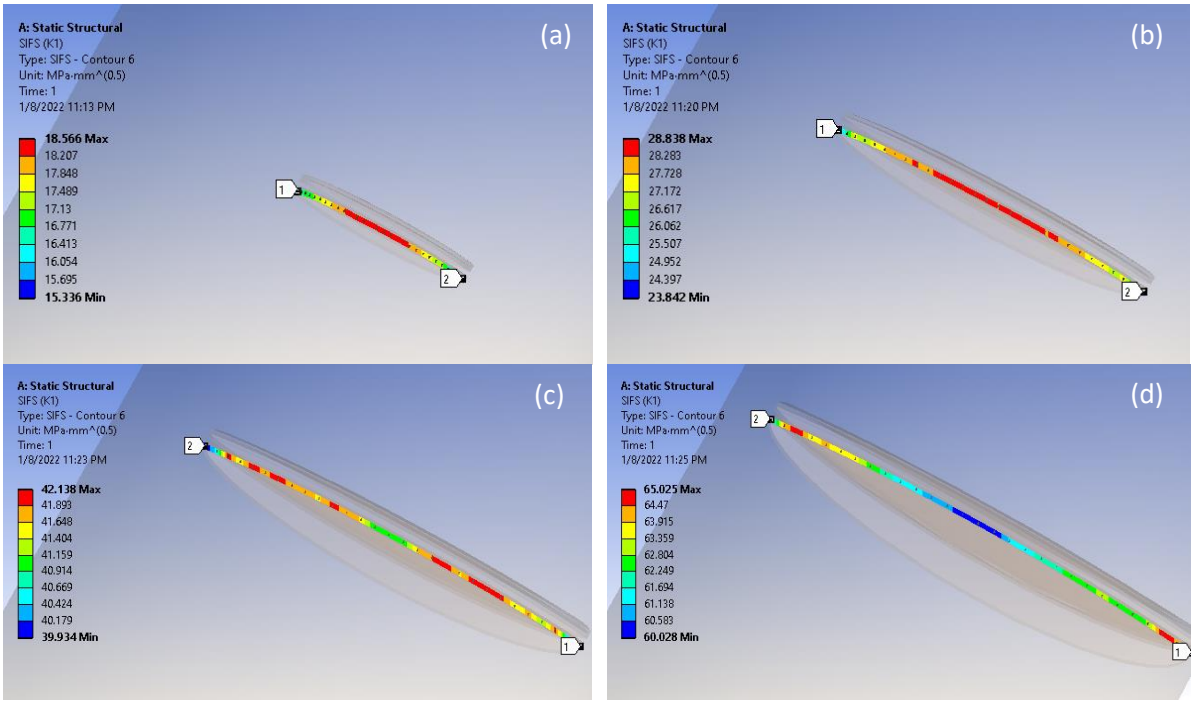

Figure 7. The stress intensity factors of tension (a) when a/D=0.1, a=5, and b=8.333, (b) when a/D=0.2, a=10, and b=16.67, (c) when a/D= 0.3, a=15, and b=25, (d) when a/D=0.4, a=20, and b=33.33

Fig. 8 illustrates the normalized stress intensity factors (SIFs), Ft, for an external semi-elliptical crack under tension loading, plotted in terms of normalized coordinates of the crack front for various values of the fracture depth ratio. The analysis focused on mode I loading, achieved by applying tension to the cylinder. Eq. 3.2 is applied to derive the tension Mode I failure, and the resulting tension force, Ft, is provided to demonstrate this failure mode.

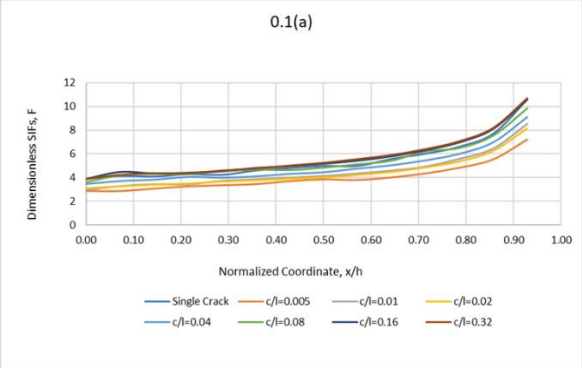

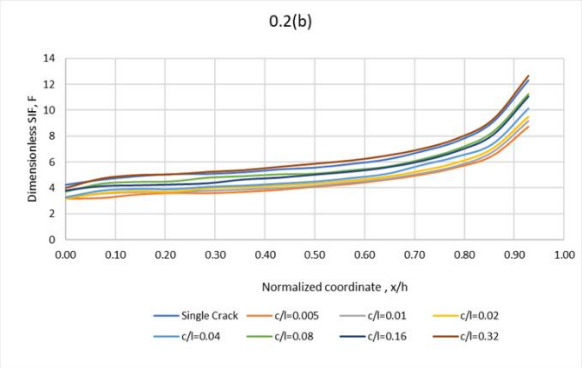

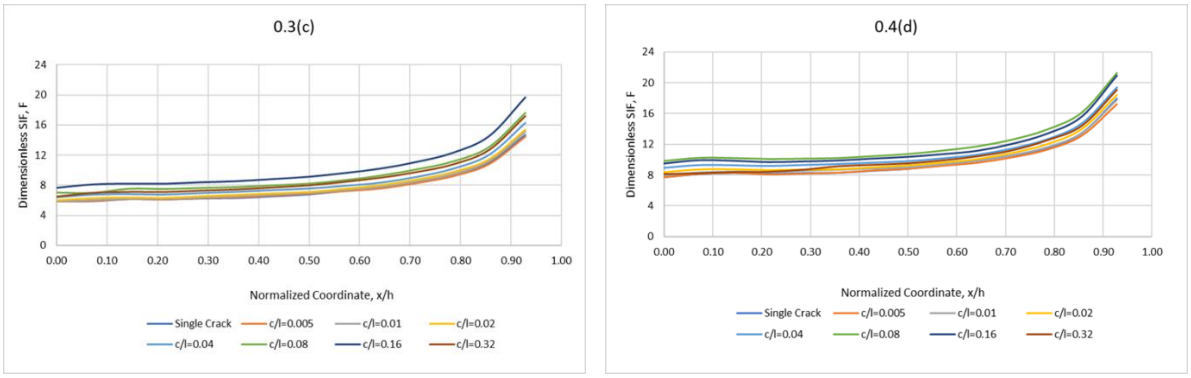

Figure 8. Dimensionless SIFs for parallel cracks under tension, a/b=0.6 and (a) a/D=0.1, (b) a/D=0.2, (c) a/D=0.3and (d) a/D=0.4

The data for all crack depth ratios studied reveal that the distribution of SIFs appears symmetrical along the fracture front, with the tension force, Ft, approaching the value for a single crack. The dimensionless SIFs are observed to increase with the fracture separation distance, a/D. When cracks are close to each other, their interaction has a more significant influence, whereas when fractures are further apart, the impact of the surrounding crack decreases. The most significant value of SIFs shifts from the maximum depth on the crack front, x/h, to the surface point, and the values tend to follow a straight line during the transition from the initial stage to the well-known transition effect. The SIFs reach their maximum value near the surface and decrease to their lowest value at the deepest point.

When the ratio of fracture separation distance, c/l, is greater than 0.08, the dimensionless SIFs values are similar to those of a single fracture. This ratio of two interacting cracks can be considered separate or single. The Ft values increase with the increasing relative crack depth ratios, indicating that as the crack increases, this leads exhibit high Ft values and vice versa. This impact of fracture depth ratio is consistent across all examples studied. It should be noted that the dimensionless SIF is affected by more than just c/l, as seen in the following graph.

Table 2 presents the interaction factor (IF) values for external parallel cracks subjected to strain with a/b = 0.6 and a/D ratios of 0.1, 0.2, 0.3, and 0.4. The maximum interaction point is observed at x/h = 0.00, as shown by the distribution of Ft values along the fracture front. As the crack separation distance, c/l, increases, the interactions between all cracks also increase. However, as the values of the crack front, x/h, increase, the interactions decrease. Parallel cracks located close to each other are more likely to interfere. Furthermore, the deeper the crack, the larger the gap needed for a fracture to remain unaffected by its surrounding crack.

Table 2: Interaction factor for parallel external cracks under tension when a/b=0.6

a/D = 0.1							
	Ψ						
x/h	c/l = 0.005	c/l = 0.01	c/l = 0.02	c/l = 0.04	c/l = 0.08	c/l=0.16	c/l=0.32
0.00	0.191	0.196	0.208	0.231	0.242	0.259	0.261
0.50	0.156	0.163	0.163	0.171	0.196	0.211	0.214
0.93	0.064	0.073	0.073	0.082	0.088	0.095	0.096
a/D = 0.2							
	Ψ						
x/h	c/l = 0.005	c/l = 0.01	c/l = 0.02	c/l = 0.04	c/l = 0.08	c/l=0.16	c/l=0.32
0.00	0.176	0.177	0.175	0.180	0.203	0.209	0.219
0.50	0.135	0.133	0.139	0.143	0.163	0.161	0.188
0.93	0.057	0.060	0.063	0.067	0.071	0.071	0.086
a/D = 0.3							
	Ψ						
x/h	c/l = 0.005	c/l = 0.01	c/l = 0.02	c/l = 0.04	c/l = 0.08	c/l=0.16	c/l=0.32
0.00	0.099	0.099	0.102	0.109	0.119	0.130	0.134
0.50	0.150	0.152	0.155	0.165	0.178	0.199	0.209
0.93	0.066	0.069	0.071	0.075	0.081	0.090	0.095

a/D = 0.4							
	Ψ						
x/h	c/l = 0.005	c/l = 0.01	c/l = 0.02	c/l = 0.04	c/l = 0.08	c/l=0.16	c/l=0.32
0.00	0.130	0.134	0.140	0.151	0.166	0.182	0.188
0.50	0.114	0.116	0.119	0.127	0.139	0.152	0.159
0.93	0.054	0.055	0.058	0.060	0.066	0.073	0.077

3.2 Interaction Analysis for Single and Multiple Parallel Cracks of Bending

The solid shaft is subjected to a bending force of 3000Nm using Ansys Finite Element Software under various geometrical parameters as shown in Fig. 9. The interactions of surface cracks on the solid shaft are analysed, with different crack depths and lengths along the Z-axis, considering a reference crack at Z=1 or a separation distance of c/l=0.005.

Fig.10 illustrates the normalized SIFs, Fb, for a circumferential crack located on the outer surface of a cylinder under bending loading. The normalized coordinates of the crack front are used to plot the distribution of Fb for various fracture depth ratios. The bending Mode I of failure is analysed using Eq 3.3, and the resulting bending force, Fb, is used to demonstrate this failure mode. The values of Fb are found to be relatively insensitive to the crack separation distance (c/l) since Fb is generated by a bending moment rather than a tensile force. However, as the crack separation distance increases, the interaction between various cracks becomes more significant. The curves of Fb are similar to each other, and they become closer together as the fracture depth ratio a/D increases. However, some interaction values are far apart, especially when a/D is less than 0.3 and x/h is less than 0.5. This could be due to the closure of cracks along the crack front, which is not expected for deeper fractures. The dimensionless SIFs reach their maximum value at c/l=0.04 and decrease to their minimum value at c/l=0.32. The most significant value of Fb shifts from the maximum depth on the crack front, x/h, to the surface point, and the values tend to follow a straight line during the transition from the introductory stage to the well-known transition effect. The SIFs have their maximum value close to the surface and decrease to their lowest value at the deepest point.

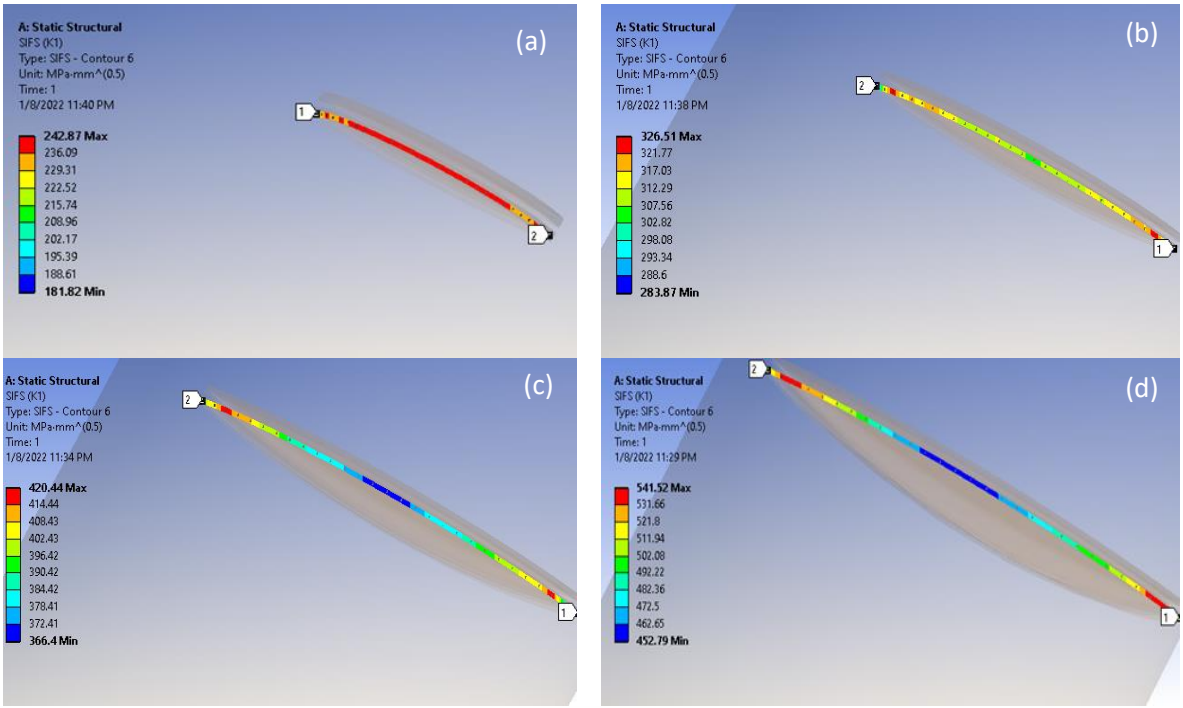

Figure 9. The stress intensity factor of tension (a) when a/D=0.1, a=5, and b=8.333, (b) when b= a/D=0.2, a=10, and b=16.67, (c) when a/D= 0.3, a=15, and b=25, (d) when a/D=0.4, a=20, and b=33.33.

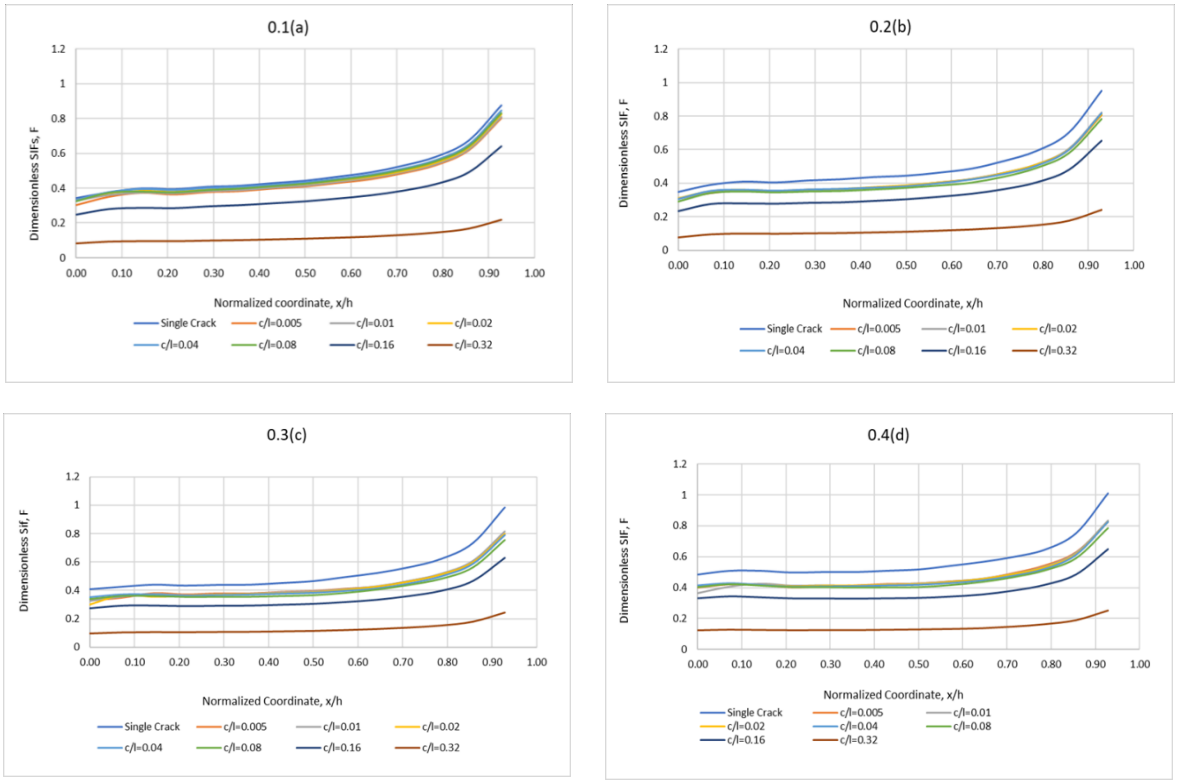

Figure 10. Dimensionless SIFs for parallel cracks under bending, a/b=0.6 and (a) a/D=0.1, (b) a/D=0.2, (c) a/D=0.3 and (d) a/D=0.4.

Table 3 displays the interaction factor between two parallel crack configurations under a bending force. It can be observed that point x/h=0.00 exhibits significant interaction in crack depth ratios a/D of 0.1 and 0.2, as indicated by the interaction factor values. As the fracture depth increases, the interaction effect becomes more pronounced, while the opposite is true for shallower cracks. The interactions between all cracks increase with an increase in crack separation distance, represented by c/l. However, as the crack front values, x/h, increase, the interactions between the cracks decrease.

Table Error! No text of specified style in document. : Interaction factor for parallel external cracks under bending when a/b=0.6

a/D = 0.1							
	Ψ						
x/h	c/l = 0.005	c/l = 0.01	c/l = 0.02	c/l = 0.04	c/l = 0.08	c/l=0.16	c/l=0.32
0.00	2.564	2.770	2.810	2.810	2.737	2.097	0.710
0.50	2.087	2.112	2.167	2.210	2.166	1.656	0.567
0.93	1.048	1.059	1.080	1.107	1.087	0.840	0.288
a/D = 0.2							
	Ψ						
x/h	c/l = 0.005	c/l = 0.01	c/l = 0.02	c/l = 0.04	c/l = 0.08	c/l=0.16	c/l=0.32
0.00	2.596	2.567	2.571	2.545	2.414	1.949	0.646
0.50	1.956	1.969	1.961	1.937	1.888	1.548	0.564
0.93	0.889	0.904	0.894	0.903	0.863	0.719	0.264
a/D = 0.3							
	Ψ						
x/h	c/l = 0.005	c/l = 0.01	c/l = 0.02	c/l = 0.04	c/l = 0.08	c/l=0.16	c/l=0.32
0.00	1.971	1.949	1.794	2.107	2.031	1.646	0.586
0.50	1.956	1.969	1.961	1.937	1.888	1.548	0.564

0.93	0.889	0.904	0.894	0.903	0.863	0.719	0.264
a/D = 0.4							
Ψ							
x/h	c/l = 0.005	c/l = 0.01	c/l = 0.02	c/l = 0.04	c/l = 0.08	c/l=0.16	c/l=0.32
0.00	1.971	1.949	1.794	2.107	2.031	1.646	0.586
0.50	1.822	1.811	1.777	1.764	1.687	1.411	0.534
0.93	0.819	0.840	0.823	0.814	0.778	0.650	0.251

3.3 Interaction Analysis for Single and Multiple Parallel Cracks of Torsion

The stress intensity factors KI, KII, and KIII for semi-elliptical surface cracks are determined using the same method as for tension and bending stress. To compare the data obtained under different loading conditions, torsion stresses of Ts=3000Nm are applied. At the maximum fracture depth, the cracks exhibit pure Mode II and Mode III conditions (KI=0), similar to the behaviour observed for Mode I under tension and bending stress loading.

For two parallel external cracks subjected to pure torsional stress, only Ftor-II and Ftor-III could be calculated, showing that the SIFs for mode II and mode III are identical when applied to a cylinder as shown in Fig. 11 and 13. As a result, there is no interaction between Mode I and the other Modes. The orientation of the normalized SIFs as a function of the normalized crack front position, x/h, for modes II and III is shown in Fig. 12, and equations are used to obtain the normalized SIF values for torsion modes II and III.

Fig. 12 shows the normalized SIF distribution, FtorII, for parallel external cracks under tension loading with a/b = 0.6. The torsion force, Ftor-II, is presented to demonstrate the torsion mode II failure derived using Eq (3.3). At the crack's deepest point, x/h=0.00, Ftor-II achieves its maximum Dimensionless SIFs and then decreases until it reaches zero at the deepest point on the fracture surface by moving towards the intersection between the front of the crack and the outside surface of the cylinder shaft. The Torsion Mode II force is determined separately for each crack separation distance, indicating double cracks interaction with this type of force. When a/D is increased, no significant changes in the curve are observed along the fracture front. In all graphs, it can be seen that the Dimensionless SIFs value decreases linearly with the crack separation distance and normalized coordinates or crack front.

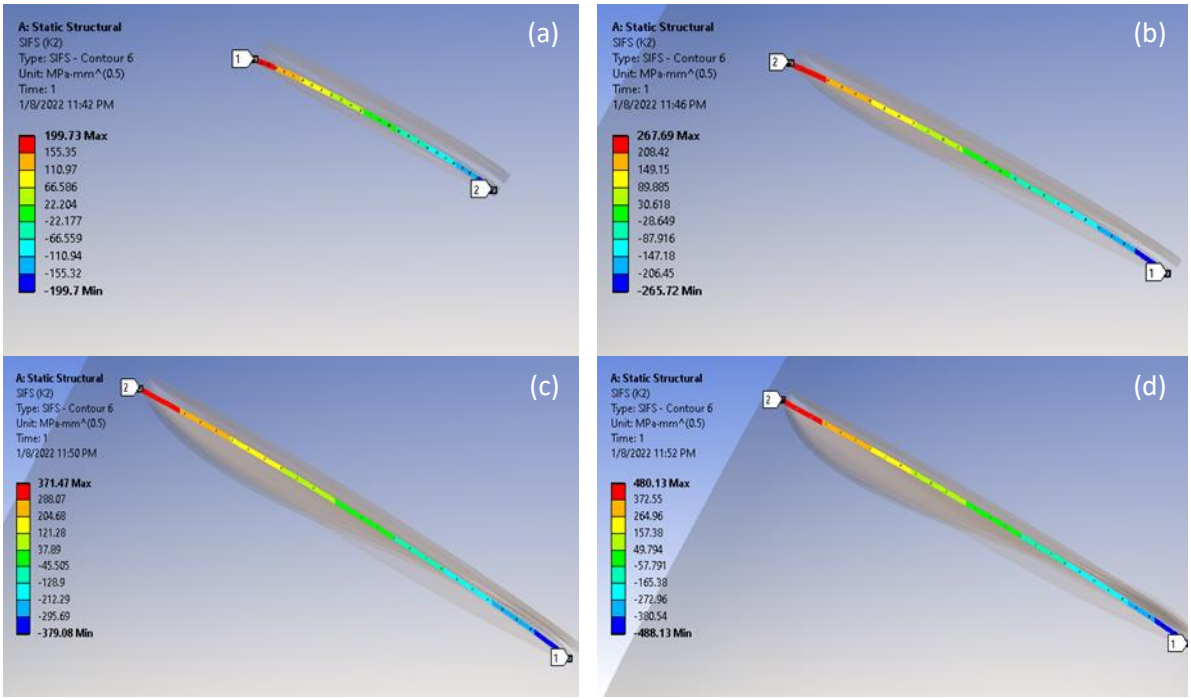

Figure 11. The stress intensity factor of torsion mode II when (a) a/D=0.1, a=5, and b=8.3333, (b) when a/D=0.2, a=10, b=16.67, when (c) a/D 0.3, a=15, and b=25 and when (d) a/D=0.4, a=20, and b=33.33

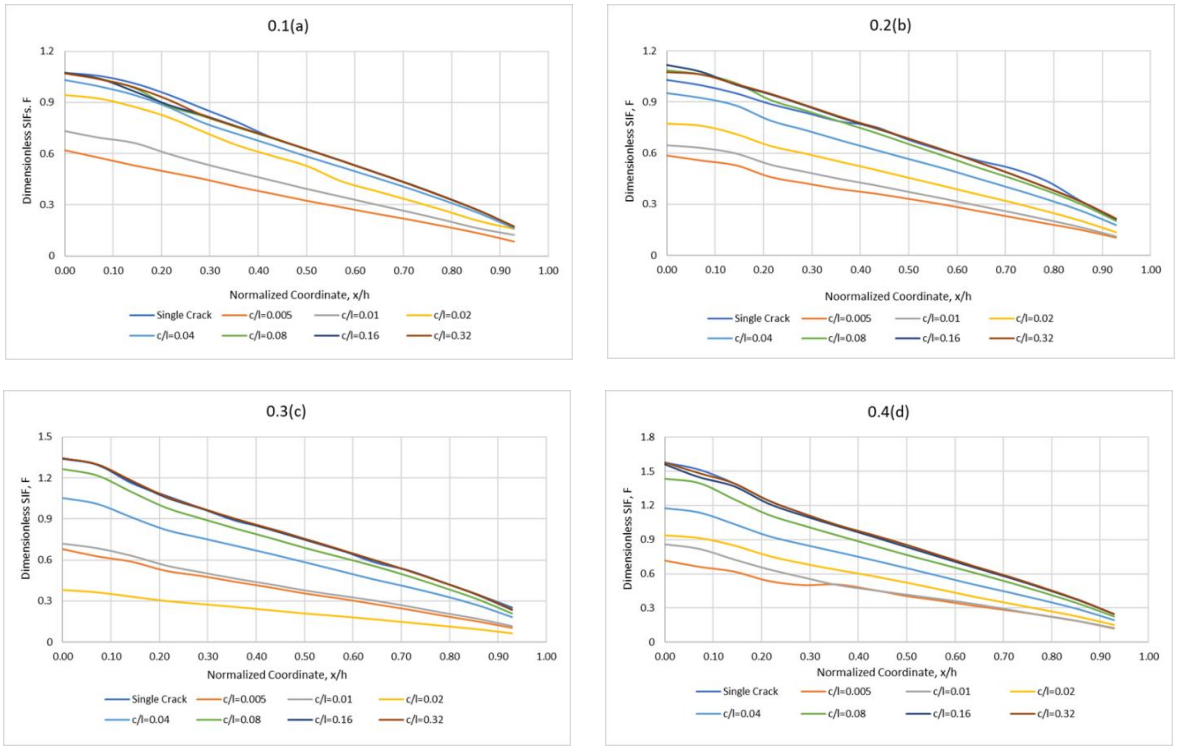

Figure 12. Dimensionless SIFs for parallel cracks under torsion Mode II, a/b=0.6 and (a) a/D=0.1, (b) a/D=0.2, (c) a/D=0.3 and (d) a/D=0.4

Table 4 presents the interaction factor between parallel fractures in mode II Torsion failure, FTor-II. The table shows the shielding effect of FTor-II on Mode II parallel fractures, which has minor interaction effects. Until the two fractures diverge sufficiently and separate, even a small c/l significantly affects all of the evaluated a/D. At a/D=0.1, the fracture is amplified at the deepest and shallowest regions, but at a/D=0.2, 0.3, and 0.4, the crack behaves more like a shield.

Table 4: Interaction factor for parallel external cracks under mode II when a/b=0.6

a/D = 0.1							
				Ψ			
x/h	c/l = 0.005	c/l = 0.01	c/l = 0.02	c/l = 0.04	c/l = 0.08	c/l=0.16	c/l=0.32
0.00	0.538	0.637	0.782	0.896	0.933	0.933	0.931
0.50	0.828	1.008	1.263	1.489	1.593	1.599	1.602
0.93	2.863	3.481	4.416	5.356	5.693	5.755	5.750
a/D = 0.2							
				Ψ			
x/h	c/l = 0.005	c/l = 0.01	c/l = 0.02	c/l = 0.04	c/l = 0.08	c/l=0.16	c/l=0.32
0.00	0.376	0.415	0.497	0.611	0.696	0.717	0.717
0.50	0.722	0.811	0.995	1.231	1.425	1.492	1.493
0.93	1.588	1.692	2.113	2.722	3.139	3.259	3.310
a/D = 0.3							
				Ψ			
x/h	c/l = 0.005	c/l = 0.01	c/l = 0.02	c/l = 0.04	c/l = 0.08	c/l=0.16	c/l=0.32
0.00	0.377	0.399	0.212	0.586	0.704	0.746	0.747
0.50	0.722	0.811	0.995	1.231	1.425	1.492	1.493
0.93	1.613	1.862	1.002	2.869	3.309	3.689	3.786
a/D = 0.4							
				Ψ			

x/h	c/l = 0.005	c/l = 0.01	c/l = 0.02	c/l = 0.04	c/l = 0.08	c/l=0.16	c/l=0.32
0.00	0.289	0.321	0.378	0.474	0.578	0.629	0.635
0.50	0.555	0.571	0.717	0.891	1.052	1.145	1.170
0.93	1.944	2.012	2.449	3.134	3.699	3.992	4.026

Fig. 14 shows the normalized SIF value for an exterior crack in Torsion Mode III, where identical values of a/D and a/b are used for this specific external fracture. The behaviour is essentially similar to Torsion Mode II, and the transition effect can be observed. Higher SIF values are attained when the relative crack depth ratio is high, whereas SIF values decrease as the relative crack depth ratio increases. This behaviour is established for an external crack. The ratio of relative crack depth affects the external crack, and as the fracture separation distance increases, the Dimensionless SIFs for all crack depth ratios increases. The size of the relative fracture depth, represented by the ratio a/D, has a substantial influence on the behaviour of FTorIII. If a/D is less than 0.3, the maximum FTorIII begins at the fracture front's deepest point. When a/D is greater than 0.3, the maximum FTorIII is relocated to the particle's exterior. It can be observed that when x/h = 0.30, the highest FTorIII and the lowest FTorIII shift positions. As a result of this x/h displacement, FTorIII is now more irregularly distributed along the crack front. This is because the shaft exposed to torsion moments benefits from deeper fractures when a/b = 0.6.

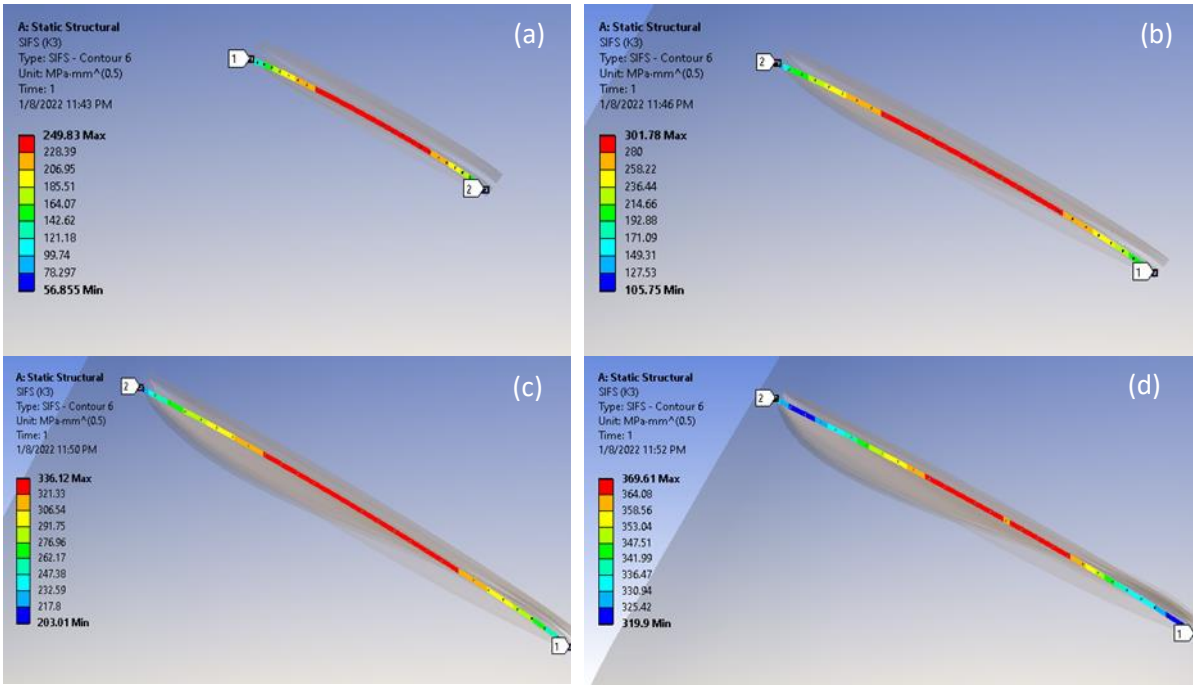

Figure 13. The Stress Intensity Factor of Torsion Mode III when (a) a/D=0.1, a=5, and b=8.3333, when (b) a/D=0.2, a=10, and b=16.67, when (c) a/D=0.3, a=15, and b=25 and when (d) a/D=0.4, a=20, and b=33.33

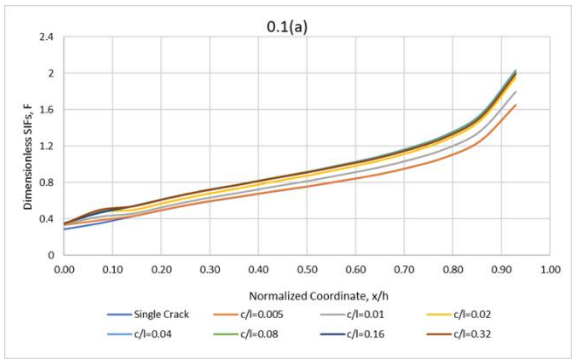

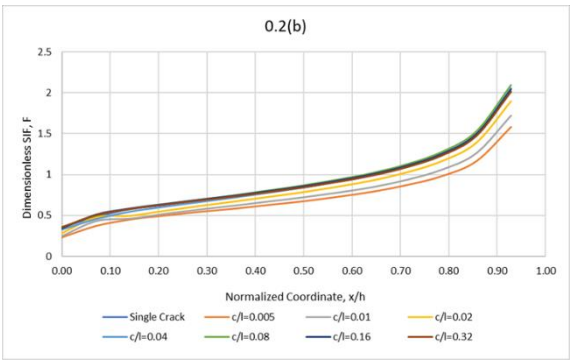

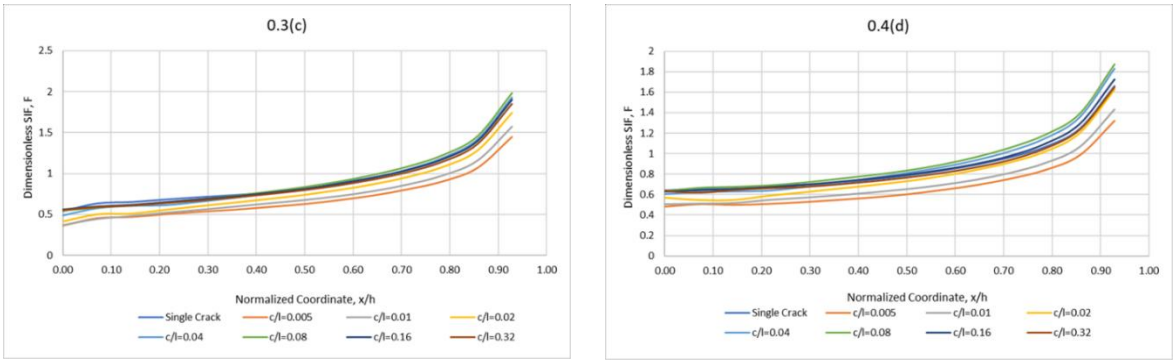

Figure 14. Dimensionless SIFs for parallel cracks under torsion Mode III, a/b=0.6 for (a) a/D=0.1, (b) a/D=0.2, (c) a/D=0.3 and (d) a/D=0.4

Table 5 presents the external parallel interaction factor for Torsion Mode III. It is observed that the interaction effect is most significant at a c/l ratio of 0.08 and x/h of 0.00 when a/D ratios are 0.1, 0.2, 0.3, and 0.4. This demonstrates that the crack depth has a substantial impact on the interaction rate, while a higher a/D ratio increases the interaction effect. The transition x/h occurs when a/b reaches the outer edge of the bar, indicating that various fracture evolutions could be achieved during the crack development process.

Table 5: Interaction factor for parallel external cracks under mode III when a/b=0.6

a/D = 0.1							
	Ψ						
x/h	c/l = 0.005	c/l = 0.01	c/l = 0.02	c/l = 0.04	c/l = 0.08	c/l=0.16	c/l=0.32
0.00	1.952	2.383	2.841	3.127	3.164	3.147	3.150
0.50	1.328	1.430	1.543	1.610	1.613	1.601	1.598
0.93	0.608	0.661	0.720	0.748	0.742	0.734	0.733
a/D = 0.2							
	Ψ						
x/h	c/l = 0.005	c/l = 0.01	c/l = 0.02	c/l = 0.04	c/l = 0.08	c/l=0.16	c/l=0.32
0.00	1.794	1.909	2.192	2.558	2.790	2.794	2.782
0.50	0.941	1.011	1.097	1.181	1.218	1.197	1.183
0.93	0.389	0.424	0.467	0.507	0.516	0.503	0.496
a/D = 0.3							
	Ψ						
x/h	c/l = 0.005	c/l = 0.01	c/l = 0.02	c/l = 0.04	c/l = 0.08	c/l=0.16	c/l=0.32
0.00	1.249	1.272	1.413	1.655	1.877	1.918	1.892
0.50	1.612	1.739	1.896	2.075	2.148	2.087	2.043
0.93	0.402	0.436	0.483	0.536	0.550	0.528	0.513
a/D = 0.4							
	Ψ						
x/h	c/l = 0.005	c/l = 0.01	c/l = 0.02	c/l = 0.04	c/l = 0.08	c/l=0.16	c/l=0.32
0.00	0.758	0.793	0.885	1.049	1.205	1.243	1.229
0.50	0.983	1.067	1.189	1.318	1.355	1.292	1.244
0.93	0.478	0.519	0.588	0.661	0.677	0.625	0.596

3.4 Interaction Analysis for Combined Loading

Previous studies have demonstrated that determining stress intensity factors (SIFs) in the presence of combined loadings can be challenging [13]. However, the superposition method has been suggested as a possible solution for normalizing each SIF, particularly for comparable loading modes such as Mode I [14]. Before the fractures are repaired, the influence of mixed-mode loading on external parallel cracks is investigated. In this configuration, the shaft is subjected to simultaneous forces of tension, bending, and torsion. To obtain normalized SIFs for

mixed-mode loading, an equation is developed to determine equivalent SIFs, denoted as FEqv. Each type of loading results in a distinct form of damage to the structure, hence FEqv is used to express the normalized SIFs for mixed-mode loading. The same geometry, which is a shaft with a semi-elliptical surface crack, is used to calculate FEqv by applying Eq 3.5. The KI, KII, and KIII stress intensity components are determined using the same methodology as previous studies.

The distribution of FEqv for external, parallel fractures is depicted in Fig. 15. The distribution of FEqv near the fracture front is identical for tension and bending loads. It is observed that the FEqv-Ext value changes as the crack depth ratio varies, even when the aspect ratio, a/b, remains constant. The ratio of x/h to a/D is proportional. In general, the trend of all graphs is slightly convex when they reach x/h>0.70.

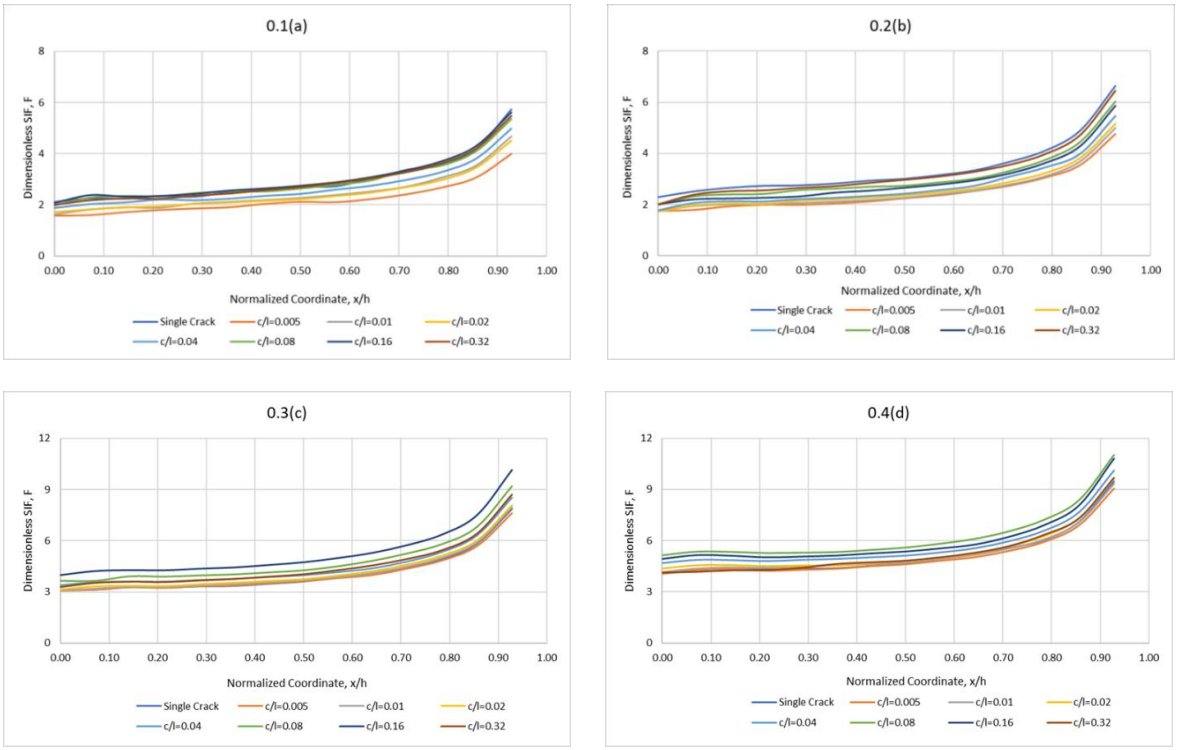

Figure 15. Dimensionless SIFs for external parallel cracks under mixed-mode loading, a/b=0.6

Table 6 presents the interaction factor for external parallel cracks under mixed-mode loading. The FEqv distribution along the crack front shows that the highest value occurs at the deepest point of the fracture, x/h = 0.00. As the crack separation distance, c/l, increases, the interaction effect becomes more significant. This implies that the interaction between fractures is influenced by their distance from each other. In particular, fractures with a high a/D ratio need to be sufficiently far apart from other surrounding cracks to be considered safe from their interaction impact.

Table 6: Interaction factor for parallel external cracks under combined loading when a/b=0.6

a/D = 0.1							
	Ψ						
x/h	c/l = 0.005	c/l = 0.01	c/l = 0.02	c/l = 0.04	c/l = 0.08	c/l=0.16	c/l=0.32
0.000	0.357	0.367	0.389	0.427	0.445	0.464	0.449
0.500	0.291	0.303	0.304	0.318	0.360	0.378	0.368
0.930	0.122	0.137	0.137	0.152	0.163	0.172	0.167
a/D = 0.2							
	Ψ						
x/h	c/l = 0.005	c/l = 0.01	c/l = 0.02	c/l = 0.04	c/l = 0.08	c/l=0.16	c/l=0.32
0.000	0.330	0.331	0.328	0.336	0.375	0.379	0.382
0.500	0.252	0.250	0.260	0.266	0.301	0.292	0.329
0.930	0.108	0.113	0.117	0.124	0.132	0.131	0.151
a/D = 0.3							

				Ψ			
x/h	c/l = 0.005	c/l = 0.01	c/l = 0.02	c/l = 0.04	c/l = 0.08	c/l=0.16	c/l=0.32
0.000	0.188	0.189	0.193	0.207	0.224	0.243	0.245
0.500	0.277	0.282	0.286	0.303	0.326	0.360	0.371
0.930	0.123	0.129	0.131	0.138	0.148	0.164	0.169
a/D = 0.4							
				Ψ			
x/h	c/l = 0.005	c/l = 0.01	c/l = 0.02	c/l = 0.04	c/l = 0.08	c/l=0.16	c/l=0.32
0.000	0.242	0.247	0.261	0.279	0.306	0.332	0.336
0.500	0.213	0.217	0.222	0.235	0.257	0.279	0.287
0.930	0.101	0.104	0.108	0.113	0.123	0.135	0.140

4.0 CONCLUSION

In this study, finite element analysis is conducted on a solid cylinder shaft to calculate stress intensity factors (SIFs) for semi-elliptical parallel surface fractures with varying crack geometrical parameters. The objective is to determine the interaction factor between single and double cracks by normalizing the SIFs for tension, bending, torsion, and mixed-mode loading. The results show that the behaviour of multiple cracks is influenced by their geometrical parameters and loading types.

For tension loading, the graph shows that as the crack distance increases, multiple cracks present a similar trend to a single crack. However, for bending loads, the double cracks do not approach the single crack value as the separation distance increases. Surprisingly, for torsion in mode II, the dimensionless stress intensity steadily decreases as the crack front ratio increases, whereas in mode III, the double cracks tend to attain a similar pattern to the single crack as the ratio of crack distance increases. For mixed-mode loading, only a minor change is observed as the ratio of crack distance increases.

The examination of parallel crack orientations revealed that crack interaction might be in the form of amplification and shielding or no interaction. The study found that the shielding effect is present for all fracture geometry characteristics analysed, and cracks interact with one another more frequently around their outermost region than at their deepest point. The majority of shielding effects occur on the outside point rather than at the deepest point.

The findings of this study have important implications for identifying and predicting cracks in solid shafts, particularly in marine shafts, to reduce any failure and avoid catastrophic incidents. However, some results are different from previous research, and future studies should consider including thermal loads such as pressure and vibration analysis to enhance the analysis of multiple surface crack interaction on the shaft.

ACKNOWLEDGEMENT

The authors would like to express their gratitude to the MVS Supply & Services Sdn. Bhd, Kuala Terengganu for the opportunity of Industrial attachment that gave valuable insights for the simulation work carried out. Also, special thanks to Nor Shahida Najiha bt Rosli for fasilitating Ansys Simulation.

REFERENCES

[1] MAN Diesel &Turbo, “Basic Principles of Ship Propulsion,” *Man Diesel & Turbo*, 2011. http://www.mandieselturbo.com/files/news/filesof5405/5510_004_02 low.pdf

[2] C. Sleeter, “December, 2012,” *NSPS Shipbuild. Value Chain.*, no. September 2015, pp. 213–219, 2015,

[3] M. M. Muhammad, M. S. D. Yati, N. H. Nik Yusoff, and M. C. Isa, “Fracture Failure Analysis of a Marine Propeller Shaft,” *Def. S T Tech. Bull.*, vol. 13, no. 2, pp. 240–246, 2020.

[4] G. Vizentin, G. Vukelić, and M. Srok, “Common failures of ship propulsion shafts,” *Pomorstvo*, vol. 31, no. 2, pp. 85–90, 2017,

[5] N. Sachs, “Failure Analysis Of Machine Shafts,” *Maintenance Technology*, 2012. https://www.efficientplantmag.com/2012/07/failure-analysis-of-machine-shafts/

[6] D. Chandra, J. Purbolaksono, and Y. Nukman, “Surface crack growth in a solid cylinder under combined cyclic bending-torsion loading,” *ARPN J. Eng. Appl. Sci.*, vol. 13, no. 3, pp. 1033–1041, 2018.

[7] M. M. Hamdan, M. K. Awang, and A. E. Ismail, “Double Surface Cracks Interaction on Cylindrical Rod

Under Tensile and Torsional Loading," vol. 1, pp. 69–77, 2020.

[8] M. K. Awang, A. E. Ismail, A. L. Mohd Tobi, and M. H. Zainulabidin, "Stress intensity factors and interaction of two parallel surface cracks on cylinder under tension," *IOP Conf. Ser. Mater. Sci. Eng.*, vol. 165, no. 1, pp. 1–10, 2017,

[9] R. Citarella, V. Giannella, M. Lepore, and G. Dhondt, "Dual boundary element method and finite element method for mixed-mode crack propagation simulations in a cracked hollow shaft," *Fatigue Fract. Eng. Mater. Struct.*, vol. 41, no. 1, pp. 84–98, 2018,

[10] A. E. Ismail, A. K. Ariffin, S. Abdullah, and M. J. Ghazali, "Stress intensity factors for surface cracks in round bar under single and combined loadings," *Meccanica*, vol. 47, no. 5, pp. 1141–1156, 2012,

[11] A. Syahmi, M. K. Awang, A. E. Ismail, and M. N. Ibrahim, "Interaction of Surface Crack on Solid Shaft Due to Combined Loading," vol. 1, pp. 117–135, 2021.

[12] J. J. Sinou and A. W. Lees, "The influence of cracks in rotating shafts," *J. Sound Vib.*, vol. 285, no. 4–5, pp. 1015–1037, 2005,

[13] M. de Fonte, E. Gomes, and M. de Freitas, "Stress intensity factors for semi-elliptical surface cracks in round bars subjected to mode I (bending) and mode III (torsion) loading," *Eur. Struct. Integr. Soc.*, vol. 25, no. C, pp. 249–260, 1999,

[14] A. E. Ismail, A. K. Ariffin, S. Abdullah, M. J. Ghazali, M. Abdulrazzaq, and R. Daud, "Stress intensity factors under combined bending and torsion moments," *J. Zhejiang Univ. Sci. A*, vol. 13, no. 1, pp. 1–8, 2012,